Remote Sensing of Environment 126 (2012) 51–61

Contents lists available at SciVerse ScienceDirect

Remote Sensing of Environment

journal homepage: www.elsevier.com/locate/rse

Atmospheric correction of MERIS data for case-2 waters using a neuro-variational inversion

Julien Brajard [a,b,*], Richard Santer [a], Michel Crépon [b], Sylvie Thiria [b]

[a] ULCO, MREN, av. Foch, Wimereux 62930, France
[b] LOCEAN, BC100, T45-55, pl. Jussieu, Paris 75005, France

ARTICLE INFO

Article history:
Received 9 January 2009
Received in revised form 14 May 2012
Accepted 10 July 2012
Available online 5 September 2012

Keywords:
Remote sensing
Atmospheric correction
Case 2 waters
Coastal waters
MERIS
NeuroVaria
Variational inversion
Neural networks
Ocean color

ABSTRACT

One of the difficulties in analyzing the ocean signal provided by satellite ocean color sensors is that it is strongly polluted by atmospheric contributions, which should be removed by an atmospheric correction process.

We propose a new methodology, based on spectral optimization in the near-infrared, to simultaneously estimate the contributions generated by atmospheric signals and oceanic particles, which is valid for case-1 and case-2 waters. This approach, denoted NeuroVaria, combines a neural network to model the radiative transfer with a variational algorithm for the spectral inversion.

NeuroVaria was applied to MERIS data recorded between August 2003 and September 2005 over the Adriatic Sea, off the Venice Lagoon, for which, in situ measurements of the water-leaving reflectance and aerosol optical thickness were available. We present comparisons between the results obtained using NeuroVaria and the MERIS second reprocessing (Megs7.4), and those derived from in situ measurements. We show that NeuroVaria achieves better estimations of the aerosol optical properties, and improves the atmospheric correction for case-2 waters. Using MERIS multi-spectral images, it was thus possible to detect typical features of the Po River discharge into the northern Adriatic, as well as suspended sediments due to the shoaling of wind waves on their approach to the seashore shallow waters.

1. Introduction

Since 1997, several ocean-color sensors, such as SeaWiFS (NASA's Sea-viewing Wide Field-of-view Sensor), MODIS (Moderate Resolution Imaging Spectroradiometer), the French CNES's POLDER (Polarized and Directionality of the Earth's Reflectance), and MERIS (the European Space Agency's Medium Resolution Imaging Spectrometer), have been launched on satellites. They were mainly designed to analyze the optical properties of case-1 waters, which depend on the intrinsic properties of the water itself and those of the phytoplankton and the other associated constituents (Morel & Prieur, 1977). On the contrary, the optical properties of case-2 waters (which are mainly coastal) are characterized by the presence in the water of colored, dissolved organic matter and suspended particulate matter whose concentrations are uncorrelated with those of phytoplankton. The case-2 waters present characteristics that make them difficult to analyze (Sathyendranath, 2000). The first is that they are highly variable in space and time. The sensors should present a good spatial resolution and an adequate sampling frequency. For that purpose, we only considered multispectral imagers that have a good coverage (one image every 2–3 days) and an adequate spatial resolution (1 km for MODIS, 300 m for MERIS). The second characteristic is that the optical properties are much more variable for case-2 waters than for case-1 waters. Therefore, the sensor should provide a large number of spectral bands of good spectral quality. It has been shown (Ruddick et al., 2006) that some useful assumptions can be made in the near-infrared part of the signal. This property was widely used in this paper. This explains why the algorithm presented in this paper uses measurements from the sensor MERIS that have 5 bands in the near-infrared (versus 3 bands for MODIS).

In the case of satellite sensors, the orbiting radiometer measures the solar flux reflected by the ocean and the atmosphere. In order to estimate the oceanic components (e.g. the chlorophyll-*a* linked to phytoplankton) or the inherent optical properties (IOP) of the ocean (e.g. marine absorption and scattering coefficients), a critical step in the processing of top-of-the-atmosphere (TOA) measurements is the so-called atmospheric correction. This involves the removal of the atmospheric contribution to the recorded signal, in order to determine the contribution of the ocean alone. Classical methods of atmospheric correction (Antoine & Morel, 1999; Gordon, 1997) are based on the assumption that the ocean is "black" in the NIR band (e.g. $\lambda > 700$ nm) after the removal of the sun glint, that is the signal recorded by the satellite in this band is due to the atmosphere alone. For case-2 waters, this assumption is no longer valid, because the presence of suspended particulate matter can have a strong impact on the return signal at NIR wavelengths. More suitable algorithms have been developed, in order

* Corresponding author at: LOCEAN, BC100, T45-55, pl. Jussieu, Paris 75005, France.
E-mail address: julien.brajard@locean-ipsl.upmc.fr (J. Brajard).

0034-4257/$ – see front matter © 2012 Elsevier Inc. All rights reserved.
http://dx.doi.org/10.1016/j.rse.2012.07.004

to apply atmospheric corrections which take the specificity of case-2 waters into account (Doerffer & Schiller, 2007). An iterative algorithm, referred to as the bright pixel atmospheric correction (BPAC) proposed by Moore et al. (1999), has been implemented in the MERIS ground segment. Similar approaches were proposed for the SeaWiFS sensor (Bailey et al., 2010; Ruddick et al., 2000). Another method doing a direct inversion of the multi-spectral TAO signal by using specific neural networks has been presented in Schroeder et al. (2007).

In the present paper we propose an algorithm based on the spectral matching principle, which uses five near-infrared wavelengths to perform the atmospheric correction for case-2 waters. This algorithm, denoted NeuroVaria, makes use of a general multi-dimensional approach that simultaneously optimizes the atmospheric and oceanic signals in the NIR. The atmospheric contribution retrieved in the NIR is then extrapolated to visible wavelengths, in order to process the atmospheric correction and to derive water-leaving reflectances at visible wavelengths.

Global spectral matching techniques have already been used to solve similar problems in ocean-color image processing, such as atmospheric correction in the presence of absorbing aerosols (Banzon et al., 2004; Brajard et al., 2006; Chomko & Gordon, 2001; Jamet et al., 2005; Moulin et al., 2001). They have also been applied to highly regionalized data reduction processes (Frette et al., 1998). A spectral optimization algorithm (SOA) was proposed by Kuchinke et al. (2009) for retrieving bio-optical parameters in case-2 waters. Although SOA and NeuroVaria are similar in principle, they present some differences: (i) NeuroVaria also performs an atmospheric correction, whereas SOA only aims at retrieving water constituents, such as chlorophyll-*a*; (ii) NeuroVaria optimizes all the parameters simultaneously, whereas SOA performs a multi-step procedure similar to that of the standard algorithm; (iii) NeuroVaria makes no regional assumptions, whereas in SOA the wavelength dependence of the oceanic signal should be specified a priori; (iv) the mathematical treatment used in the two algorithms is very different.

In the present paper, we propose a general approach to processing case-2 water images. To calibrate NeuroVaria, we used synthetic data generated with a standard optical model, together with various radiative-transfer calculations. The synthetic data were stored in large datasets referred to as Look-up-tables (LUT). NeuroVaria was then applied to MERIS images of the Adriatic Sea. Finally, in situ measurements were used to validate the retrieved images. In the first section of this paper, we present the full set of data: synthetic LUT, MERIS images, and in situ measurements. The second section describes the NeuroVaria algorithm. The third section presents the results and the validation of the method. Section 3 is devoted to a discussion and Section 4 presents some conclusions.

1.1. Data

NeuroVaria used three distinct datasets: (i) a synthetic dataset containing the optical parameters and computed with a radiative transfer code (Deuzé et al., 1989) to calibrate the algorithm; (ii) an image dataset extracted from MERIS imagery to which the NeuroVaria algorithm was applied; and (iii) an *in situ* dataset to validate the results.

1.1.1. The synthetic dataset

The optical quantity computed by the radiative transfer model is the TOA reflectance $\rho_{toa}(\lambda)$, defined by:

$$\rho_{toa}(\lambda,\theta_s)=\frac{\pi\times L_{toa}(\lambda,\theta_s)}{E_0(\lambda)\times\cos(\theta_s)}$$

where $L_{toa}(\lambda)$ is the radiance measured by the radiometer, $E_0(\lambda)$ is the extra-atmospheric solar irradiance corrected for the Sun–Earth distance and θ_s is the zenith solar angle. The signal is corrected for ozone absorption, and a standard sea-level atmospheric pressure of 1013.25 hPa is assumed.

The reflectance signal can be expanded in a simplified form (Gordon, 1997):

$$\rho_{toa}(\lambda,\theta_s,\theta_v,\Delta\varphi)=\rho_A(\lambda,\theta_s,\theta_v,\Delta\varphi)+T(\lambda,\theta_s,\theta_v)\times\rho_w(\lambda) \quad (1)$$

where ρ_{toa} is the top-of-the-atmosphere reflectance, ρ_A is the atmospheric reflectance (which is classically decomposed into three terms: the Rayleigh reflectance, ρ_r; the aerosol reflectance, ρ_a; and the coupled Rayleigh–aerosol reflectance, ρ_{ra}), ρ_w is the water-leaving reflectance, T is the total atmospheric transmittance (both upward and downward), θ_s is the zenith solar angle, θ_v is the zenith viewing angle, $\Delta\varnothing$ is the azimuth difference angle, and λ is the central wavelength.

In this paper, the effect of white caps due to weak winds is neglected in the studied region, which is considered as a test case, but could be added without any loss of generality of the algorithm. The glitter contribution is not taken into account, so the algorithm can only invert non-glint pixels that are determined from the relative positions of the sensor and the sun.

In order to process the images presented in Section 1.1.2, we generated synthetic atmospheric look-up tables (LUTs) for ρ_A and T using the 13 central wavelengths of MERIS (see Table 1), and an oceanic LUT for ρ_w using only the 5 NIR wavelengths.

Atmospheric LUTs: LUT-A and LUT-T. The successive order radiative-transfer code (Deuzé et al., 1989) was used to generate the two atmospheric LUTs: LUT-A for ρ_A and LUT-T for T. These datasets depend mainly on the optical properties of the aerosols. Table 2 presents the different configurations used to generate LUT-A and LUT-T. A Junge power law was used to represent the size distribution of the aerosols. Note that, for this initial version of the case-2 water algorithm, the aerosols are restricted to the non-absorbing type, meaning that the single scattering albedo is: $\omega_o=1$. The choice of aerosol models is discussed in Section 4.1 and a sensitivity study is presented in Appendix A.

The oceanic dataset LUT-O. The remote water-leaving reflectance ρ_w is expressed by (Ruddick et al., 2006):

$$\rho_w(\lambda)=R\times\frac{a_w(\lambda_0)}{a_w(\lambda)}\times\left(\frac{\lambda}{\lambda_0}\right)^{-\gamma} \quad (2)$$

where λ_0 is a reference wavelength, R is a simplified notation for $\rho_w(\lambda_0)$, a_w is the absorption by the water and γ is a shape parameter that depends on the size of the particles (Lee, 2003). Values of a_w were taken from Pope and Fry (1997) and Kou et al. (1993). In this work, λ_0 is equal to 709 nm.

This expression is valid in the near-infrared bands (e.g. $\lambda>700$ nm). Some approximations and assumptions were made (Ruddick et al., 2006). The absorption by other constituents than the water itself is assumed to be negligible, which has an effect less than 1% on ρ_w in the spectral range 700 nm–900 nm. The temperature and salinity dependency, which can lead to an error of 9% at 740 nm for a 12 °C difference in temperature, is also neglected. Finally, this expression should be modified for extremely clear waters ($\rho_w(780)<0.0001$) and for extremely turbid waters ($\rho_w(780)>0.1$). Modeling clear waters is not relevant in an atmospheric correction process and extremely turbid

Table 1
Central wavelengths of the MERIS sensor (rounded).

λ (nm)												
Visible								Near-infrared (NIR)				
412	443	490	510	560	620	665	681	709	754	779	865	885

Table 2
Description of LUT-A.

Parameter	Values	Notes
Atmospheric pressure	1013.25 hPa	
Wind speed, w_s	3 m/s and 7.2 m/s	
Refractive index, m	1.35	
θ_s, θ_v	From 0° to 60°	24 Gauss quadrature angles
$\Delta\phi$	From 0° to 180°	25 regularly spaced values
AOT[a] τ at 550 nm,	From 0 to 1	11 regularly spaced values
Junge size parameter, ν	From 2.5 to 5.5	31 regularly spaced values
Wavelengths	From 412 nm to 885 nm	13 values (see Table 1)

[a] AOT is the Atmospheric Optical Thickness.

waters are beyond the scope of this paper. Therefore, Eq. (2) is expected to be valid in a large variety of situations. It should be noted that the model was made using simplified hypotheses, none of which made any use of a priori knowledge of the studied region.

Using Eq. (2), realistic water-leaving reflectances can be simulated with a dependence on two parameters only: an intensity parameter, R; and a shape parameter, γ. A reference table LUT-O for $\rho_w(\lambda)$ ($\lambda > 700$ nm) is generated with R values ranging from 0 to 0.09 and γ values from -0.2 to 2.2. The range of parameter values has been adjusted according to the International Ocean Colour Coordinating Group (IOCCG) recommendations (Lee, 2003).

1.1.2. The satellite dataset

The NeuroVaria algorithm, which is described in detail in Section 2, was used to process spatial reduced resolution images measured by the Medium Resolution Imaging Spectrometer (MERIS), which is a multi spectral radiometer carried by the Envisat satellite, launched in 2002 by the European Space Agency (ESA). The radiometric measurements were corrected for ozone absorption, and a correction was made so that a standard atmospheric pressure of 1013.25 hPa could be assumed. Our study focused on images taken in the northern Adriatic Sea (44°N–46°N, 12°E–14°E), between August 2003 and November 2005. In order to avoid glitter contamination, we considered only the left-hand sides of the images. Finally, pixels identified by MERIS as being GLINT_RISK, SUSPECT, BRIGHT, COASTLINE, or INVALID were excluded from the dataset. Following these selection criteria, only 39 images were retained.

1.1.3. The in situ dataset

The Acqua Alta Oceanographic Tower (AAOT), built in 1970, is situated 8 nautical miles off the Venice Lagoon (45.314°N, 12.508°E) and has been used to provide data for the Coastal Atmosphere and Sea Time Series (CoASTS). This region is characterized by both case-2 and case-1 water types (Berthon & Zibordi, 2007; D'Alimonte et al., 2007). To validate the NeuroVaria atmospheric correction, we focused on optical measurements of normalized water-leaving reflectances, and on the aerosol optical thickness given by the CIMEL radiometer (Zibordi et al., 2006a). These measurements were made in the context of the AERONET-OC (AErosol RObotic NETwork-Ocean Color) program (Zibordi et al., 2006b) (http://aeronet.gsfc.nasa.gov/new_web/ocean_color.html). The in situ dataset was extracted by the toolkit developed in the MERMAID (MERis MAtchup In situ Database) project. The normalized water-leaving reflectance is computed as (Gordon, 1997):

$$\rho_{wN}(\lambda) = \frac{\pi \times L_{wN}(\lambda)}{E_0(\lambda)} \tag{3}$$

where E0 is the extraterrestrial solar irradiance, LwN is the normalized water radiance and λ the central wavelength.

Table 3 shows the range of values applicable to the parameters used in this paper, between August 2003 and November 2005. Since the selected data needed to be matched with each of the 39 selected MERIS images, a total of 39 measurements could be used in the validation. The Angstrom coefficient α was computed using the following expression:

$$\alpha\left(\lambda_i, \lambda_j\right) = -\log\left(\frac{\tau(\lambda_i)}{\tau\left(\lambda_j\right)}\right) / \log\left(\frac{\lambda_i}{\lambda_j}\right) \tag{4}$$

For an aerosol-free atmosphere, this coefficient has a negligible influence on the atmospheric reflectance spectrum, so that α is computed only for $\tau(870) > 0.05$ in the following.

Table 3
Measured values at the AAOT site from August 2003 to November 2005.

Parameter	Min. value	Max. value	Average	Standard deviation
$\rho_w(412)$	3.80×10^{-3}	3.05×10^{-2}	1.49×10^{-2}	6.7×10^{-3}
$\rho_w(443)$	6.20×10^{-3}	3.86×10^{-2}	1.90×10^{-2}	8.4×10^{-3}
$\rho_w(490)$	9.10×10^{-3}	4.76×10^{-2}	2.60×10^{-2}	1.1×10^{-2}
$\rho_w(560)$	1.07×10^{-2}	5.51×10^{-2}	2.35×10^{-2}	1.1×10^{-2}
$\tau(870)$	1.03×10^{-2}	0.22	6.37×10^{-2}	5.48×10^{-2}
$\alpha(555,870)$	0.10	2.08	1.37	0.54

2. Application of NeuroVaria to case-2 waters

The NeuroVaria algorithm was first developed to provide accurate atmospheric corrections in all atmospheric situations, including cases with absorbing aerosols (Brajard et al., 2006) whose optical properties cannot be solely deduced from the near-infrared part of the signal. The first important characteristic of NeuroVaria is that it makes a multispectral optimization, by taking into account simultaneously several spectral bands to estimate several optical properties. On the contrary, standard algorithms perform a series of unidimensional calculations. Therefore, NeuroVaria allows the inverse problem to be solved in cases for which the atmospheric and oceanic contributions cannot be determined separately from specific spectral bands. That is why a first use of NeuroVaria was to perform atmospheric correction with absorbing aerosol whose optical properties mainly depend on the visible part of the signal ($\lambda < 700$ nm). This characteristic is used in the present work to estimate simultaneously oceanic and aerosol parameters in the near-infrared part of the signal. A major advantage of NeuroVaria is its ability to process a variational inversion, using a second-order gradient-descent algorithm well adapted for estimating a large number of parameters of a complex model. It relies on the same theory as that used for variational data assimilation applied in operational meteorology and which has been well developed in the last three decades (Talagrand & Courtier, 1987). In the present case, the control parameters are the aerosol (ν and τ) and oceanic (R and γ) optical parameters, the model is the radiative-transfer code and the outputs are the water-leaving reflectances at several wavelengths.

The algorithm minimizes a cost function $\boldsymbol{J}$ (described in Section 2.4) by adjusting the relevant atmospheric and oceanic parameters (ν,τ, R, γ), the so-called control parameters. $\boldsymbol{J}$ describes the difference between the satellite measurement and a simulated reflectance computed using Eq. (1), together with the specifications of the LUT-O, LUT-A and LUT-T datasets. Fig. 1 describes the complete process, followed by the variational inversion. The various considerations needed to calibrate NeuroVaria are described in the following. Appendix B gives an overview of more operational aspects of NeuroVaria.

2.1. The multilayer perceptrons

Fig. 1 shows that an important step in the inversion procedure is the simulation of reflectances by the direct model. This simulation is made by the successive order radiative-transfer code, which implies lengthy and costly computations. An efficient way to overcome this

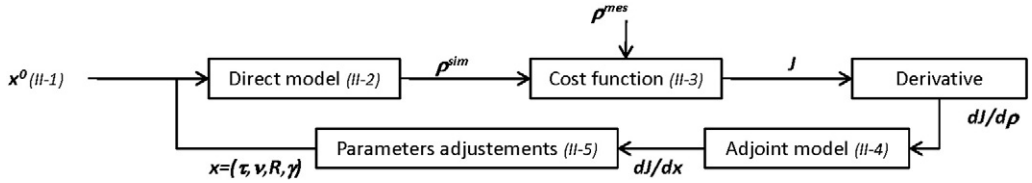

Fig. 1. Schematic diagram of the variational inversion. The italic numbers refer to the label of the subsection where the step of the variational inversion is detailed.

difficulty is to model this code by an MLP (multi-layer perceptron), which is a specific class of artificial neural networks dedicated to the modeling of non-linear functions. MLPs are continuous differentiable functions, well suited to representing the direct model in variational estimations. Artificial neural networks have also been successfully applied to the modeling of inverse functions in geophysical applications (Thiria et al., 1993). In the present work, MLPs were also used to estimate a first-guess value of the aerosol parameters τ and υ by inverting the satellite sensor measurements. A brief introduction to these mathematical objects is given in the following.

An MLP is a set of elementary functions (here, a sigmoid function) that are combined using connections associated with different weights. It has been shown that MLPs are universal, non-linear interpolators; i.e. that they can approximate any continuous function (Bishop, 1995). The elementary functions are the so-called neurons. In the present problem, we used multilayered networks formed by several layers of neurons. Multilayered architecture has one layer receiving input, one layer broadcasting output and one or more intermediate layers (the hidden layers) situated in between.

The sizes of the input and the output layers are determined by the size of the problem itself. The values of the weights of the connection and the number of hidden neurons (i.e. number of neurons in the hidden layers) are determined after an optimization procedure, the so-called learning phase. This optimization is made using a dataset containing representative samples of the input/output values of the neural network. At the end of this learning phase, the MLP can be used to simulate any output, from an input belonging to the range of validity defined during the learning phase. It produces a differentiable function with respect to the input of the neural network.

2.2. The first guess

To initiate the inversion procedure, a first estimation of the control parameters is needed. The first guess has to be sufficiently close to the true value to improve the efficiency of the minimizing procedure and the accuracy of the finally retrieved values.

To a first order, we assumed that the aerosol parameters τ and υ could be estimated independently, using the top-of-the-atmosphere reflectance spectrum in the near-infrared. The oceanic contribution, which is non-negligible in case-2 waters, is fixed to a median value corresponding to average case-2 waters. The intensity parameter R is set to 0.001 and a common value is used for the shape parameter γ ($\gamma=1$) (Sydor et al., 2002). Following the methodology described by Jamet et al. (2004), τ and υ were estimated with MLPs. These two MLPs are shown in Fig. 2.

During this phase, these two MLPs estimating τ and υ, the so-called MLP-TAU and MLP-NU, were learned separately using a subset of the previously described LUTs. A training dataset of 150 000 simulations of ρ_{toa} was randomly extracted from the LUT-A and LUT-T datasets. Table 4 provides the description, architecture and performance of these MLP, computed from a dataset of 20 000 samples, all of which were independent of the training dataset. It should be noted that the performance of the estimation of υ was computed for $\tau>0.05$. For $\tau<0.05$, the aerosol model was assumed to have negligible influence, and υ was set to 4.

2.3. The direct model

The direct model (radiative-transfer equations) used in the cost function $\boldsymbol{J}$ (see Fig. 1) is represented by two other MLPs modeling the different terms of Eq. (1). One is dedicated to the simulation of ρ_A (denoted by MLP-A) and the other to T (MLP-T). A sub-dataset of 150 000 values of ρ_A (respectively T) was randomly extracted from LUT-A (respectively LUT-T), in order to calibrate MLP-A (respectively MLP-T). The resulting MLPs are shown in Fig. 3.

An independent dataset of 20 000 elements was used to evaluate the performance of these MLPs. Table 5 provides their description, architecture and performance. The performance of these MLPs was highlighted for wavelengths corresponding to the near-infrared part of the signal, since the minimization was performed only in the near-infrared (709 nm–885 nm). The performance for visible wavelengths ($\lambda<700$ nm) was given here to evaluate the accuracy of the extrapolation done in a second step described in Section 2.6.

The associated errors were also computed for each of the MERIS wavelengths. It can be seen that there is no correlation between the MLP errors and wavelength. The MLPs are assumed to be sufficiently accurate to correctly simulate the radiative-transfer process. The use of MLPs to simulate the direct model is a major originality of NeuroVaria, as compared with other spectral matching algorithms. Such an approach enables a quick simulation of the direct model, associated with any atmospheric situation corresponding to the range of values covered by the LUT.

2.4. The cost function

The theory of variational data assimilation is based on the minimization of a cost function, which represents the a posteriori error of the retrieved control parameters. In the present case, the expression of this cost function is:

$$J(\tau,\upsilon,R,\gamma)=\sum_{i=1}^{5}s_i\left[\rho_{toa}^{mes}(\lambda_i)-\rho_{toa}^{sim}(\lambda_i,\tau,\upsilon,R,\gamma)\right]^2+\beta^{\tau}\left(\tau-\tau^0\right)^2 +\beta^{\upsilon}\left(\upsilon-\upsilon^0\right)^2+\beta^{R}\left(R-R^0\right)^2+\beta^{\gamma}\left(\gamma-\gamma^0\right)^2 \quad (5)$$

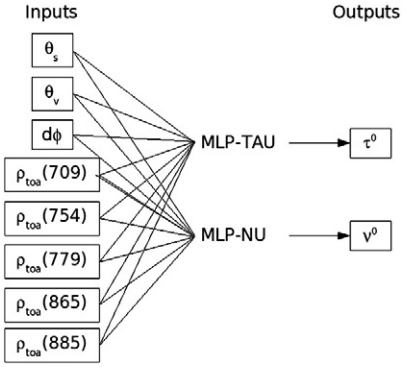

Fig. 2. Representation of the two MLPs computing the first guess values of the retrieved parameters and used to initiate the inversion. The architecture and performance of these MLPs are presented in Table 4.

Table 4
Description of MLP-TAU and MLP-NU.

MLP	MLP-TAU	MLP-NU
Inputs (8 neurons)	ρ_{toa}(709,754,779,865,885),θ_s,θ_v,$d\varphi$	
Output (1 neuron)	τ^0	ν^0
Number of hidden layers	2	2
Size of the 1st hidden layer	30	30
Size of the 2nd hidden layer	25	25
RMS[a]	1.58×10^{-2}	3.79×10^{-2}
Relative error[b]	2.77%	0.6%
r^{2}[c]	1.0	1.0

[a] Root mean square error.
[b] Relative error.
[c] Correlation coefficient.

Table 5
Description of MLP-A and MLP-T.

MLP	MLP-A	MLP-T
Inputs	θ_s,θ_v,$\Delta\phi$,λ ,τ,ν	θ,λ ,τ,ν
Output	ρ_{atm}	T
Number of hidden layers	2	1
Size of the 1st hidden layer	28	16
Size of the 2nd hidden layer	34	–
RMS[a] for $\lambda\geq708$ nm	1.43×10^{-3}	6.9×10^{-4}
Relative error[b] for $\lambda\geq708$ nm	1.11%	0.04%
r^{2}[c]	0.998	1.0
	RMS (rel. err.)	RMS (rel. err.)
$\lambda=709$ nm	1.4×10^{-3} (1.1%)	6.3×10^{-4} (0.04%)
$\lambda=754$ nm	1.5×10^{-3} (1.0%)	4.8×10^{-4} (0.04%)
$\lambda=779$ nm	1.5×10^{-3} (1.1%)	5.2×10^{-4} (0.03%)
$\lambda=865$ nm	1.2×10^{-3} (1.2%)	9.7×10^{-4} (0.04%)
$\lambda=885$ nm	1.4×10^{-3} (1.2%)	7.4×10^{-4} (0.04%)
λ=412 nm to 681 nm (visible)	*1.8×10^{-3} (0.8%)*	*6.9×10^{-4} (0.04%)*

[a] Root mean square error.
[b] Relative error.
[c] Correlation coefficient.

where τ^0, ν^0, R^0 and γ^0 are the first-guess values for the parameters τ, ν, R and γ determined in Section 2.2, and λ_i represents the five near-infrared wavelengths given in Table 1.

The first term of $\boldsymbol{J}$ represents the error with respect to the observations of ρ_{toa}, whereas the β terms represent the errors with respect to the background values of the control parameters. Note that, in this case, the notion of "error in the observations" includes several realities: the error of the sensor itself, the error of the model used (type of aerosols, bio-optical model, ancillary parameters) and the error in the numerical simulation of the model. In the present case, we assumed the sensor errors to be small in comparison to the errors produced by the model and the numerical simulation. The weight coefficients $\boldsymbol{s}_i$ (respectively β^x) are the diagonal terms of the inverse of the variance–covariance matrix of the errors on the observation (respectively on the background). With this simplifying formulation, this matrix is diagonal, implying that the errors are uncorrelated. In this time independent problem, we identified the background terms with the first guesses.

The purpose of the present paper is to show that, even in the presence of errors in the radiative transfer model, the inversion methodology can substantially improve the atmospheric correction. Table 6 summarizes the weighting coefficients we used, which were determined taking into account the expected accuracy of the first guess, the direct simulation (Tables 4, 5), and the outcome of experiments run with synthetic data. Fundamentally, the coefficients s and β determine the relative importance of the model terms of the cost function with respect to the background terms. Coefficients s, which are the most important in this study, are used to adjust the control parameters so as to constrain the simulated observations to fit the actual ones. The coefficients β are used to ensure that the retrieved parameters stay close to the background values, which are assumed to be close to the true values. This criterion is particularly important for the estimation of the parameters τ and ν, which are accurately initialized with MLPs (see Section 2.2). Note that, even if there are no a priori values for the oceanic parameters, the coefficients β are not zero (since this would correspond to the case for which there is no a priori knowledge). In this particular case, the two coefficients β^R and β^ν are used as regularization terms: in some situations (e.g. case-1 waters), the sensitivity of

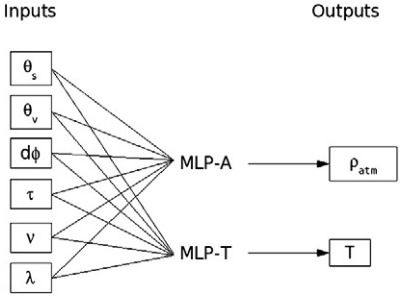

Fig. 3. Representation of the two MLPs used to simulate the direct model. The architecture and performance of these MLPs are provided in Table 5.

ρ_{toa} in the NIR to R and γ is very low, such that there is no objective criterion for the estimation of these parameters. In order to ensure that very small numerical errors in the calculation of the gradient have no impact on the retrieval of R and γ, the coefficients β^R and β^γ are used in this case to constrain the control parameters to be close to their initial values ($R=0.001$ and $\gamma=1$), throughout the inversion process.

2.5. The adjoint code

The aim of the NeuroVaria algorithm is to determine a set of control parameters (τ,ν,R,γ) that minimizes $\boldsymbol{J}$. For this, a necessary condition is to verify that:

$$\nabla J(\tau,\upsilon,R,\gamma)=0.$$

where the derivate of $\boldsymbol{J}$ with respect to a control parameter x (x being τ,ν,R or γ) is:

$$\frac{\partial J}{\partial x}=2\sum_{i=1}^{5}s_i\frac{\partial\rho_{toa}^{sim}(\lambda_i,x)}{\partial x}\left[\rho_{toa}^{mes}(\lambda_i)-\rho_{toa}^{sim}(\lambda_i,x)\right]+2\beta^x\left(x-x^0\right) \quad (6)$$

In practice, minimizing algorithms uses the gradient (Eq. 6) of $\boldsymbol{J}$ to adjust the control parameters. The key step in this process is the calculation of the expression:

$$M^*\left(\rho_{toa}^{mes}-\rho_{toa}^{sim}\right)=\frac{\partial\rho_{toa}^{sim}(\lambda_i,x)}{\partial x}\left[\rho_{toa}^{mes}(\lambda_i)-\rho_{toa}^{sim}(\lambda_i,x)\right] \quad (7)$$

where $\boldsymbol{M^*}$ is referred to as the adjoint model.

The theoretical basis of the computation of the adjoint of a code is described in Talagrand and Courtier (1987) in the context of data assimilation. Here, the computation of the adjoint code of the MLPs in Eq. (7) was done by using the classical gradient back-propagation algorithm for MLPs (Bishop, 1995) together with a specific software tool called YAO (Badran et al., 2008) which makes this procedure semi-automatic. One of the advantages of combining the use of

Table 6
Values of the weighting parameters in the cost function.

Parameter	value	σ[a]	λ	Parameter	value	σ[a]
s_1	2×10^5	2.2×10^{-3}	709	β^τ	100	0.1
s_2	2×10^5	2.2×10^{-3}	754	β^ν	10	0.3
s_3	2×10^5	2.2×10^{-3}	779	β^R	0.1	3.2
s_4	2×10^5	2.2×10^{-3}	865	β^γ	0.1	3.2
s_5	2×10^5	2.2×10^{-3}	885			

[a] Standard deviation of the error (inverse of the parameter value).

MLPs with variational inversion is that it relies on this simplified procedure to calculate the adjoint model.

2.6. The minimizing procedure

Parameter adjustment is achieved with the help of a minimizing algorithm provided by the French research agency INRIA (Institut National de Recherche en Informatique et en Automatique). This algorithm, named M2QN1, takes parameter boundaries into account and uses the BFGS (Broyden–Fletcher–Goldfarb–Shanno) formula at each iteration (Gilbert & Lemaréchal, 1989). After this iterative process, NeuroVaria produces optimized control parameters τ^{opt}, ν^{opt}, R^{opt} and γ^{opt}, in addition to various intermediate ones such as ρ_{atm}, ρ_w in the near-infrared bands. After this first process, the quantities ρ_{atm} and T are calculated at each visible wavelength (412–560 nm) using MLP-A and MLP-T (Fig. 3) starting from the geometry and the two aerosol parameters τ^{opt} and ν^{opt}. The expected accuracy of this computation is given in Table 5 (last line). The water-leaving reflectance for visible wavelengths is then computed using Eq. (1):

$$\rho_w(\lambda) = \frac{\rho_{toa}^{mes}(\lambda,\theta_s,\theta_v,\Delta\varphi) - \rho_A(\lambda,\theta_s,\theta_v,\Delta\varphi)}{T(\theta_s,\theta_v)} \quad (8)$$

3. Results

3.1. Results from a MERIS image

To illustrate the performance of NeuroVaria for case-2 waters, we selected two MERIS images, taken on 13 August 2002 and 16 August 2002. During this period, the River Po discharged absorbent dissolved substances and sediments into the Adriatic Sea, which had an impact on the water-leaving reflectance. Since the seawater beyond the river delta is typical of case-2 waters, it provides a good test for the NeuroVaria algorithm. In Fig. 4 the different regions of interest discussed in the following, are shown together with the location of the Venice observation tower (AAOT).

Fig. 5 shows the NeuroVaria retrievals on 13 August 2002, compared with those produced by the second MERIS reprocessing, Megs7.4, for three parameters: the water-leaving reflectances at 490 nm and 709 nm, which are direct outputs from the atmospheric correction, and the aerosol optical thickness, which provides an indication of the aerosol concentration in the atmosphere. The level-2 flags LAND, CLOUD, ICE_HAZE, HIGH_GLINT, MEDIUM_GLINT were applied.

According to the two algorithms, the analyzed satellite images correspond to a relatively clear day, with very few aerosols, except for some regions near to 13°E (Fig. 4, location **A** on 13 August 2002), which may have corresponded to the presence of thin clouds. These two days therefore provide a relatively simple test for the processing of case-2 water algorithms.

Firstly, the Megs7.4 MERIS retrieval produces some unrealistic noisy patterns of water-leaving reflectances at 490 nm and 709 nm (Fig. 4: location *B* on 13 August 2002), which are typical of MERIS level-2 products and do not exist in the NeuroVaria products. Secondly, some of the MERIS water reflectances appear to be correlated with the aerosol optical thickness, which generally indicates a weakness in the atmospheric correction (Fig. 4: location *C* on 13 August 2002). These correlations do not exist, or are much weaker, in the NeuroVaria $\rho_w(490)$ image. Finally, we notice that, in the lower left part of the $\rho_w(490)$ images (Fig. 5), both algorithms give very low values for $\rho_w(490)$, corresponding to the very absorbant waters resulting from the discharge of the River Po into the Adriatic Sea. The NeuroVaria retrieval shows a well-identified pattern, which could be the signature of an oceanic eddy associated with an instability of the buoyancy flow produced by the River Po discharge into the Adriatic, as reported by Umgiesser and Bergamasco (2002) and Kourafalou (2001). Patterns of $\rho_w(490)$ in the Po delta for the 13 (Fig. 5) and 16 August obtained with the NeuroVaria processing are well visible and coherent (Fig. 6), but those obtained with the Megs7.4 MERIS are very different and less visible, which could indicate a failure in the atmospheric correction of the latter. Correlations

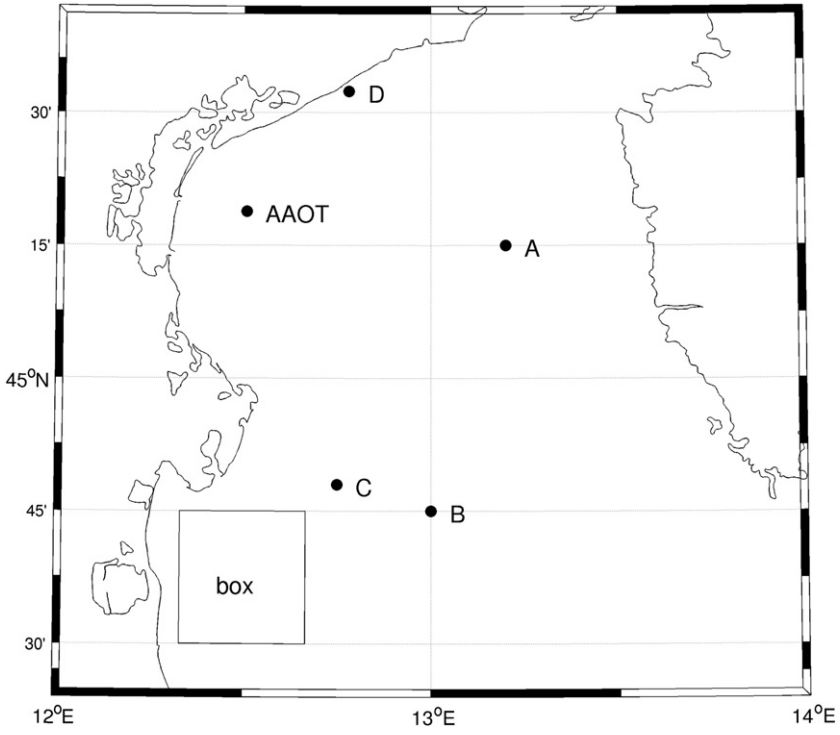

Fig. 4. Location of the different regions of interest. The box defined the region used for the time-series presented in Fig. 10.

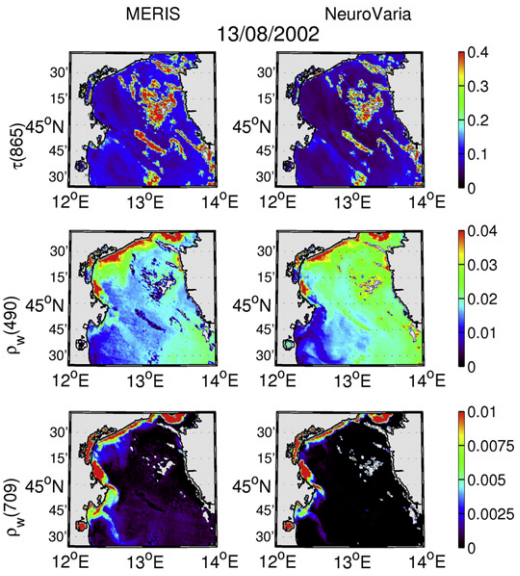

Fig. 5. MERIS (left panel) and NeuroVaria (right panel) retrievals for $\tau(865)$, $\rho_w(490)$ and $\rho_w(709)$ in the northern Adriatic Sea, on 13 August 2002. For $\tau(865)<0.35$, the correlation coefficient between $\rho_w(490)$ MERIS and NeuroVaria is 0.84.

coefficients between MERIS and NeuroVaria retrieval of $\rho_w(490)$ is 0.84 for the 13 August (Fig. 5) and 0.46 for the 15 August (Fig. 6). For the whole region, differences between MERIS and NeuroVaria retrievals of water leaving reflectance can be seen in Fig. 7. The bias is opposite in coastal waters (underestimation of $\rho_w(490)$ by NeuroVaria) as in open ocean (overestimation of $\rho_w(490)$ by NeuroVaria). Beside these bias, the general correlation of images is good and differences we noticed are clear only on small structures (see Appendix B to see a more general comparison).

The water-leaving reflectance at 709 nm generally indicates the presence of sediments, which are characteristic of case-2 waters. The two algorithms provide some very similar patterns for $\rho_w(709)$. Nevertheless, the NeuroVaria $\rho_w(709)$ values are lower than those given by the MERIS retrieval algorithm, and the River Po discharge is less visible in the $\rho_w(709)$ NeuroVaria image. This could be due to the fact that the error in the direct atmospheric model with MLP (RMS around 10^{-3}) makes the NeuroVaria algorithm less accurate at low values of water-leaving reflectance in the near-infrared. This weakness could be overcome if the atmospheric reflectance simulations were improved in the LUT dedicated to the calibration of the MLPs.

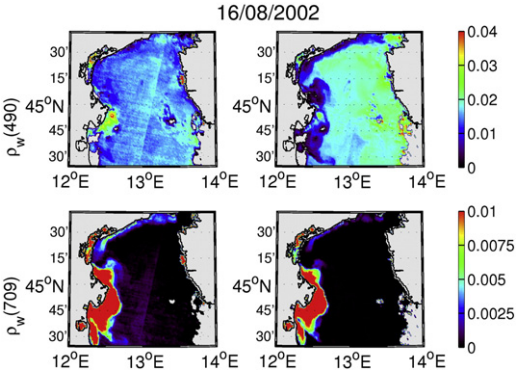

Fig. 6. MERIS (left panel) and NeuroVaria (right panel) retrievals for $\rho_w(490)$ and $\rho_w(709)$ in the northern Adriatic Sea, on 16 August 2002. The diagonal line across the image is an artefact due to the use of a different camera in the MERIS sensor which is responsible for the so-called "smile-effect" (Rast et al., 1999). For $\tau(865)<0.35$, the correlation coefficient between $\rho_w(490)$ MERIS and NeuroVaria is 0.46.

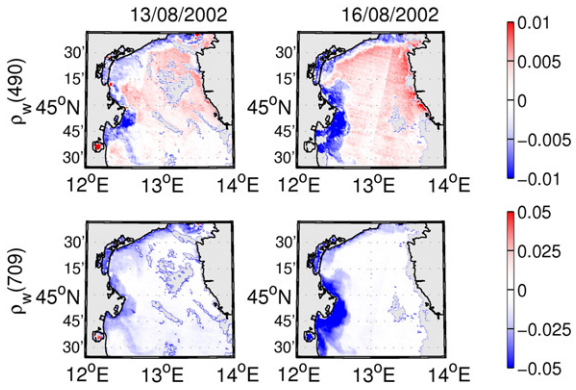

Fig. 7. NeuroVaria retrieval minus MERIS standard retrieval for $\rho_w(490)$ (upper panel) and $\rho_w(709)$ (lower panel) in the northern Adriatic Sea, on 13 August 2002 (upper panel) and on 16 August 2002 (lower panel).

It should be noted that, in the River Po discharge, the presence of particulate matter associated with low $\rho_w(490)$ values indicates the presence of highly absorbing waters containing large quantities of pigments. This is typical of the water in the River Po. On the contrary, on 13 August 2002 (Fig. 5), the high $\rho_w(490)$ values in the northern Adriatic Sea (Fig. 4, location *D*) were caused by high levels backscattering due to particles (both organic or inorganic), which could be attributed to the presence of suspended sediments assuming that water is very diffusing so that the signal does not reach the sea bottom. Nevertheless, on 16 August (Fig. 6), the same region (Fig. 4, location *D*) was found to have low $\rho_w(490)$ values, indicating the presence of absorbing waters. In Fig. 8, the bathymetric map indicates that this area corresponds to very shallow waters. The wind on 13 August 2002 was stronger than on 16 August, which may have induced a more intense suspension of sediments, generated by the shoaling of wind waves in shallow coastal waters.

3.2. Validation with the in situ dataset

The in situ measurements were compared with the Megs7.4 MERIS and the NeuroVaria products, whose retrieved images were averaged over a 9-pixel window centered on the nearest pixel to the Venice tower observation site. The match-up selection was processed according to the method proposed by (Bailey & Werdell, 2006). Comparisons were made between the remotely sensed values of water-leaving reflectance at 412 nm, 443 nm, 490 nm and 555 nm and the corresponding in situ observations. The in situ values of the aerosol optical thickness and the Angstrom exponent are available only at 555 nm and 870 nm. Therefore, comparisons were made between remotely sensed values of the Angstrom coefficients at 550 nm and 865 nm and in situ measurements of the Angstrom coefficients at 555 nm and 870 nm. Similarly, comparisons were made between remotely sensed values of the aerosol optical thickness at 865 nm and in situ measurements of the aerosol optical thickness at 870 nm. It was assumed that the Angstrom coefficient, α

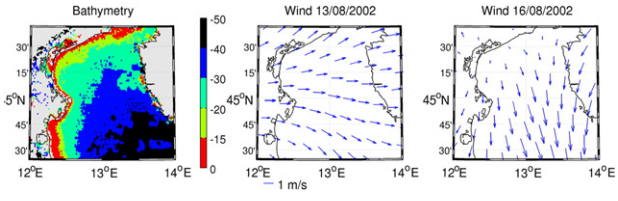

Fig. 8. Bathymetry (depth color bar in meters) of the region, and wind-velocity data on 13 August 2002 and 16 August 2002. The wind field was provided by ancillary MERIS level 1B data. It was acquired from the ECMWF (European Centre for Medium-term Weather Forecast) and was interpolated space-wise relative to the tie points.

Table 7
Statistical errors of NeuroVaria and Meris with respect to in situ measurements.

Parameter	Algorithm	RMS	Rel. error (%)	r^2
$\rho_w(412)$	NV	6.8×10^{-3}	39.8	0.18
	MER	1.2×10^{-2}	84.0	0.22
$\rho_w(443)$	NV	7.8×10^{-3}	33.8	0.33
	MER	9.2×10^{-3}	47.8	0.66
$\rho_w(490)$	NV	5.8×10^{-3}	21.6	0.79
	MER	8.3×10^{-3}	28.7	0.87
$\rho_w(560)$	NV	6.0×10^{-3}	25.7	0.90
	MER	8.0×10^{-3}	29.4	0.91
T	NV	2.9×10^{-2}	75.3	0.93
	MER	4.3×10^{-2}	99.3	0.89
A	NV	0.68	54.9	0.62
	MER	0.45	36.7	0.71

MER: standard MERIS algorithm.
NV: NeuroVaria.
RMS : root mean square error.
Rel. Error: relative error.

and the optical depth τ in Table 7 are similar for very close wavelengths. To take the influence of the bi-directionality of the water-leaving reflectance into account, ρ_w retrieved by NeuroVaria was multiplied by a tabulated, geometry-dependent coefficient (Loisel & Morel, 2001), in order to obtain normalized values of ρ_w. Table 7 shows the error statistics for all of these products, whereas Fig. 9 shows the scatter diagrams of the retrieved values versus in situ recorded values of $\tau(865)$ and $\rho_w(490)$, respectively.

It can be seen that, in terms of RMS (root mean square) and relative errors, the values determined with the NeuroVaria algorithm are systematically closer to the *in situ* measurements than those obtained using the Megs7.4 MERIS processing. The scattering of the retrieved water reflectance values (described by the correlation coefficient) increases at shorter wavelengths (412 nm and 443 nm, not shown), which denotes a strong instability in the extrapolation of near-infrared values to those relevant to visible wavelengths. This instability is somewhat stronger for the NeuroVaria algorithm and could be due to the highly simplified aerosol model used, which does not take absorption effects into account. The latter simplification is particularly significant at visible wavelengths, which could explain the observed increase in the retrieval variance in the visible bands. The effect of the aerosol model on the extrapolation procedure to the visible wavelengths is investigated in Appendix A.

The aerosol optical thickness, $\tau(865)$, is more accurate in the NeuroVaria retrieval. Note that although both algorithms overestimate the optical thickness, this effect is more significant with the MERIS algorithm. A part of this effect could be explained by the influence of the marine signal, which was incorrectly interpreted by the algorithms as an aerosol signal, leading to an increase in the apparent aerosol optical thickness. The overestimation could additionally result from the definition of the aerosol optical properties or uncertainties in the absolute calibration of the space sensor.

4. Discussion and perspectives

4.1. Aerosol models

In our model, the aerosols follow a Junge size-distribution law. The advantage of this distribution is that it is characterized by just one sizing parameter, ν, and is able to produce realistic atmospheric reflectances (Gordon, 1997). The spectral dependence of the atmospheric reflectance is characterized by a coefficient, $\varepsilon(\lambda_i,\lambda_j)$, defined by:

$$\varepsilon\left(\lambda_i,\lambda_j\right)=\frac{\omega_0(\lambda_i)\tau(\lambda_i)P_a(\theta_s,\theta_v,\Delta\varphi,\lambda_i)}{\omega_0\left(\lambda_j\right)\tau\left(\lambda_j\right)P_a\left(\theta_s,\theta_v,\Delta\varphi,\lambda_j\right)} \tag{9}$$

where $\lambda_i<\lambda_j$, ω_o is the single scattering albedo, τ is the aerosol optical thickness, and P_a is the aerosol phase function.

The aerosol description used in the present study leads to:

$$\varepsilon\left(\lambda_i,\lambda_j\right)\approx\left(\frac{\lambda_i}{\lambda_j}\right)^{3-v} \tag{10}$$

where the approximation is due to the fact that the radius of aerosol particles is limited.

In situ measurements of coastal waters (Mélin & Zibordi, 2005) suggest that the above expression of the spectral dependence could be biased at shorter wavelengths ($\lambda=412$ nm or 443 nm), leading to an overestimation of the scattering at these wavelengths. The first way to address this problem would be to include the single scattering albedo as a retrieved parameter. However, in this case, the inversion algorithm would need to be extended to the visible wavelengths. This could lead to an ill-posed problem, due to an increase in the number of control parameters, which is beyond the scope of the present study. A second solution would be to set the absorption to a value typical of the region under study. However, such an approach should be accompanied by the development of regional applications. In our study we did not consider regional solutions, which are valid only for a limited area, by demonstrating the ability of the NeuroVaria algorithm to perform accurate atmospheric corrections in a global context (see Appendix B for the conditions of application of NeuroVaria to other regions). The main effect of the simplifying assumption, that $\omega_0=1$, is to overestimate the influence of aerosol-molecule scattering at the blue end of the spectrum (412–443 nm). More details are presented in Appendix A.

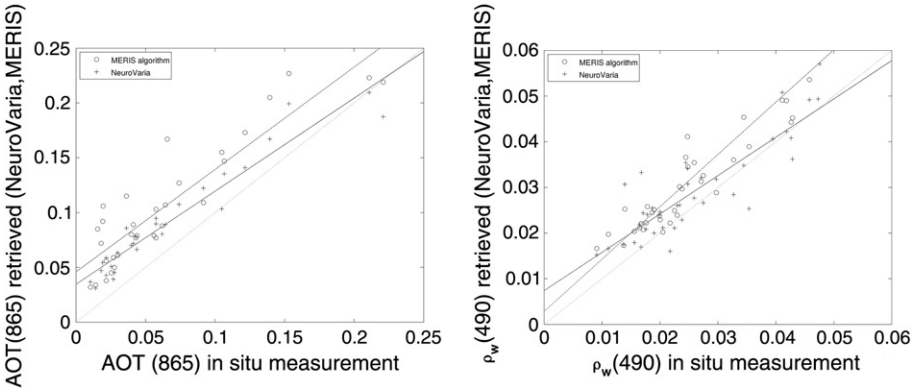

Fig. 9. Regressions of NeuroVaria (+) and MERIS (O) retrievals of $\tau(865)$ (left) and $\rho_w(490)$ (right) on the corresponding in situ measurements. The dashed lines are the corresponding linear regressions for the NeuroVaria algorithm and the solid lines are those for the MERIS algorithm. The dotted line corresponds to a theoretically perfect regression (1.0) of retrieved values with respect to in situ values.

Table 8
Description of the test dataset generated with the standard MERIS aerosol models.

Parameter	Values	Note
Model name	Rural99	Rural with 99% humidity
Atmospheric pressure	1013.25 hPa	
Wind speed, w_s	5 m/s	
θ_s,θ_v	From 0° to 60°	24 Gauss quadrature angles
$\Delta\phi$	From 0° to 180°	25 regularly spaced values
Aerosol optical thickness τ at 550 nm	0.1 and 0.2	
Angström coefficient	1.4	

4.2. Inherent optical properties (IOPs) of water

The control parameters of the inversion are the aerosol optical properties (τ and ν) and the optical properties of the ocean (R and γ). Traditionally, in ocean-color processing, water IOPs are retrieved in a second step, once the atmospheric corrections have been applied. NeuroVaria is a global approach that has the potential for simultaneously retrieving aerosol optical properties and water IOPs. As the impact of water IOPs is mainly detectable in the visible part of the signal, the inversion process would need to be extended from the near-infrared to the full spectrum (including visible wavelengths). This approach has been proposed in a previous version (Brajard et al., 2006; Brajard et al., 2008), in order to take aerosol absorption into account. Compared with the standard multi-step approach used for MERIS image inversion, NeuroVaria presents two advantages: the first is that the full inversion is based on the same model as that for the water contribution; and the second is that the global inversion avoids the propagation of errors through successive algorithmic steps. Indeed, especially in the case of highly absorptive waters, a small atmospheric correction error can lead to a significant bias in the retrieval of the optical parameters of the ocean, or may even produce negative water-leaving reflectances.

5. Conclusions

A multi-spectral optimization at five NIR wavelengths, the so-called NeuroVaria algorithm, has been proposed and adapted from previous versions (Brajard et al., 2006) in order to retrieve oceanic and atmospheric products from ocean-color images, for case-2 waters. This algorithm has been compared with the Megs7.4 MERIS algorithm and in situ measurements. In terms of RMS errors, NeuroVaria is found to provide better atmospheric corrections than the MERIS algorithm. Compared with in situ measurements, the NeuroVaria retrievals are found to be accurate and to reproduce marine structures in $\rho_w(490)$ satellite remote-sensing images, with no additional noise. Some drawbacks are also observed, in particular the underestimation of water-leaving reflectances at the shortest wavelengths (412–443 nm). We also compared (Appendix B) the weakly water leaving reflectances for the year 2009 processed with NeuroVaria to these provided by the standard MERIS algorithm (Fig. 11). The correlation between the median of NeuroVaria and MERIS retrievals is very high (0.94) showing the ability of NeuroVaria to be used for in an operational context.

An important point is that no assumptions were made concerning regional ocean and aerosol optical properties, meaning that the NeuroVaria algorithm could be applied to all case-2 waters, in theory at least. This shows that, for ocean-color remote-sensing applications, the use of a sophisticated and adapted inversion algorithm is at least as important as the modeling of complex optical properties.

Acknowledgments

The authors are grateful to Dr. G. Zibordi for providing the AERONET-OC data from the Venice site. We wish to thank ESA for providing the MERIS images, F. Zagolski for providing the radiative-transfer code, C. Mazeran and L. Bourg (from ACRIst) for their contribution to the MERIS Data Quality Working Group, and the French space agency CNES for its support. Thanks to the anonymous reviewers for their useful comments.

Appendix A. Sensitivity of NeuroVaria to the aerosol model

In order to investigate the choice of the Junge size-distribution in NeuroVaria, the sensitivity was determined by comparing the outputs of the standard aerosol models (denoted SAM) used in the MERIS processing (Antoine & Morel, 1999) to those of the NeuroVaria method. The SAM models were designed to represent the various atmospheric situations encountered in the atmospheric correction. A SAM aerosol

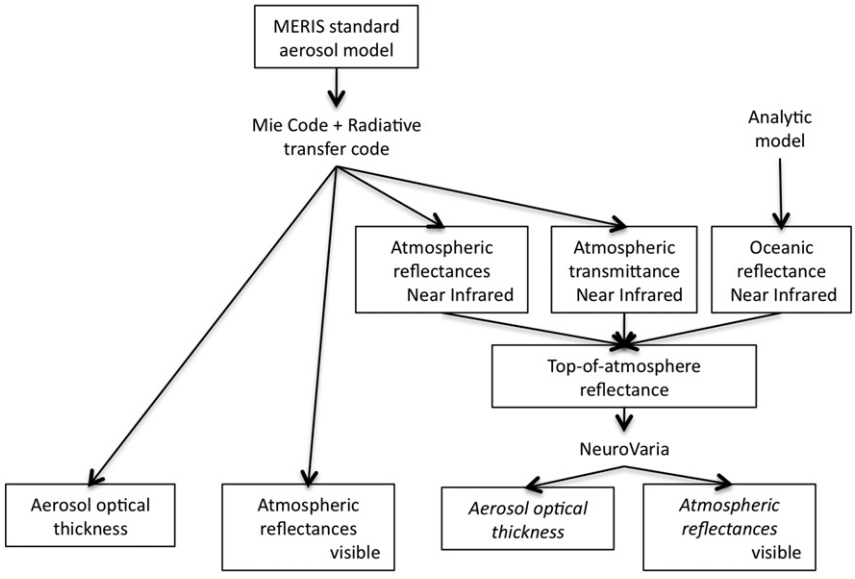

Fig. 10. Computation of NeuroVaria (italic type) and test (roman type) atmospheric reflectance and aerosol optical thickness to address the sensibility of NeuroVaria to the aerosol model.

Table 9
Statistical errors of NeuroVaria with respect to the test dataset.

Parameter	RMS	Rel. error (%)
$\rho_A(412)$	0.01	4.8
$\rho_A(443)$	7.4×10^{-3}	4.3
$\rho_A(490)$	4.7×10^{-3}	3.45
$\rho_A(560)$	4.2×10^{-3}	3.3
$\rho_A(709)$	2.6×10^{-4}	0.6
$\rho_A(865)$	1.1×10^{-4}	0.4
τ	2.0×10^{-2}	1.0
α	0.18	9.7

RMS: root mean square error.
Rel. Error: relative error.

model was determined by choosing the aerosol optical thickness and Angstrom coefficient closest to the average aerosol situation encountered in the Venice Lagoon (see Table 3). Table 8 gives a quick overview of the aerosol model selected: rural, with 99% humidity. Associated atmospheric reflectances and transmittances were then computed with the same radiative-transfer code used in this paper and then stored in a test dataset named T-dataset. Fig. 10 gives the scheme used for the generation of the T-dataset and the NeuroVaria estimations.

A comparison of the exact values given by the T-dataset and the values estimated by NeuroVaria is presented in Table 9. The errors made by NeuroVaria in the determination of the atmospheric reflectance and aerosol optical thickness were of the same order as those made in the in situ measurements (Table 7). The retrieval of the Angstrom coefficient is very accurate, which indicates that the aerosol model is correctly retrieved. As expected, the imprecision in the reflectance retrievals is larger in the blue. The shortest wavelengths (412 nm and 443 nm) are indeed more sensitive to the choice of the aerosol model and to the extrapolation procedure from the near-infrared bands to the visible bands. The error in the near-infrared is almost negligible. This shows that the principle of reproducing the signal in the near-infrared does not depend on the choice of the aerosol model. The error is therefore mainly due to the extrapolation to the visible bands and not to the minimization procedure. Using more suitable aerosol models according to the region could reduce this error. Investigating the aerosol models described in (Vidot et al., 2008) would constitute an extension of the present work. This also strongly suggests that the results could be improved by applying a minimization procedure over the entire spectrum (visible + near-infrared) if a realistic model of oceanic reflectance could be proposed for the visible wavebands in case-2 waters. Nevertheless, the increasing number of control parameters could lead to an ill-posed problem. One solution would be to assess a high Colored Dissolved Organic Matter (CDOM) concentration that would imply $\rho_w(412)\approx0$ and would allow use of the 412 nm band in the inversion.

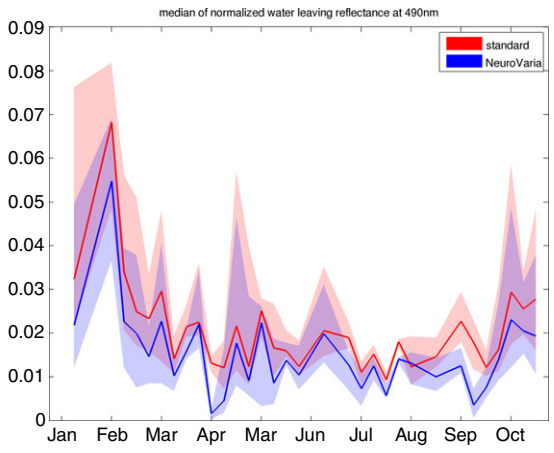

Fig. 11. Time series of the median of weekly $\rho_w(490)$ for MERIS (in red) and NeuroVaria (in blue) computing in the box defined in Fig. 4 (LAT : 44°30′N–44°45′N; LON: 12°20′E–12°40′E) for the year 2009. The correlation coefficient between MERIS and NeuroVaria retrieval is 0.94. The blue surface (resp. red surface) described the scattering of data in the box between the 10th and the 90th percentiles for the NeuroVaria retrieval (resp. MERIS retrieval).

Appendix B. NeuroVaria in an operational context

NeuroVaria was implemented in C++ language with the software YAO version 9 (free software license CECILL at http://www.cecill.info/index.en.html) and is available to any potential user by contacting one of the authors of this paper. Experiments presented in this paper were performed under Linux-Mandriva 2008 O.S. on an Intel Core 2 Quad processor (64 bits, 2.6 GHz, 4Go memory). The approximate time needed to analyze a 16 000-pixel image is 20 min (i.e. 13 pixels/s). To execute NeuroVaria for any region for which MERIS data are available, one only needs to download standard reduced-resolution MERIS level-1B data. The ancillary data needed to process images are: the wind speed, the atmospheric ozone content, and the atmospheric pressure, which are embedded in MERIS data. Some pre- and post-processing routines were coded in Matlab, but do not present any computational or theoretical difficulties. Some features should be added to the current version of NeuroVaria to deal with images with high wind speed (>10 m/s) or with ice contamination. Finally, it is possible to implement NeuroVaria in a standard processing framework (BEAM http://www.brockmann-consult.de/cms/web/beam/ or ODESA http://earth.eo.esa.int/odesa/) with only a convenient specification of inputs/outputs and a recoding of the Matlab routines. To investigate the possibilities of NeuroVaria in an operational context, the current version of NeuroVaria was used to process all available MERIS images on Northern Adriatic See during the year 2009. A time-series of weekly $\rho_w(490)$ retrieved by NeuroVaria were then compared to the standard MERIS algorithm over a "box" defined in Fig. 4. It can be noticed that, despite some differences, the correlation between the median of NeuroVaria and MERIS retrievals is very high (0.94 see Fig. 11). It confirms the ability of NeuroVaria to process a complete set of images, but the improvements that have been noticed are clearer for small structures on daily data.

References

Antoine, A., & Morel, A. (1999). A multiple scattering algorithm for atmospheric correction of remotely sensed ocean color (MERIS instrument); Principle and implementation for atmospheres carrying various aerosols including absorbing ones. *International Journal of Remote Sensing*, *20*(9), 1875–1916.
Badran, F., Berrada, M., Brajard, J., Crépon, M., Sorror, C., Thiria, T., et al. (2008). Inversion of satellite ocean colour imagery and geoacoustic characterization of seabed properties: Variational data inversion using a semi-automatic adjoint approach. *Journal of Marine Systems*, *69*(1–2), 126–136.
Bailey, S. W., Franz, B. A., & Werdell, P. J. (2010). Estimation of near-infrared water-leaving reflectance for satellite ocean color data processing. *Optics Express*, *18*(7), 7521–7527.
Bailey, S. W., & Werdell, P. J. (2006). A multi-sensor approach for the on-orbit validation of ocean color satellite data products. *Remote Sensing of Environment*, *102*, 12–23.
Banzon, V. F., Evans, R. E., Gordon, H. R., & Chomko, R. (2004). SeaWiFS observations of the Arabian Sea southwest monsoon bloom for the year 2000. *Deep-Sea Research Part II*, *51*, 189–208.
Berthon, J. -F., & Zibordi, G. (2007). Bio-optical relationships for the northern Adriatic Sea. *International Journal of Remote Sensing*, *25*, 1527–1532.
Bishop, C. M. (1995). *Neural networks for pattern recognition*. Oxford, UK: Oxford University Press.
Brajard, J., Jamet, C., Moulin, C., & Thiria, S. (2006). Use of a neuro-variational inversion for retrieving oceanic and atmospheric constituents from satellite ocean colour sensor: Application to absorbing aerosols. *Neural Networks*, *19*(2), 178–185.
Brajard, J., Moulin, C., & Thiria, S. (2008). Atmospheric correction of SeaWiFS ocean color imagery in the presence of absorbing aerosols off the Indian coast using a neuro-variational method. *Geophysical Research Letters*, *35*, 20604.
Chomko, R., & Gordon, H. R. (2001). Atmospheric correction of ocean color imagery: Test of the spectral optimization algorithm with SeaWiFS. *Applied Optics*, *40*(18), 2973–2984.
D'Alimonte, D., Zibordi, G., & Berthon, J. -F. (2007). Statistical classification of seawater bio-optical types. *IEEE Transactions on Geoscience and Remote Sensing*, *45*, 2644–2651.

Deuzé, J. L., Herman, M., & Santer, M. (1989). Fourier series expansion of the transfer equation in the atmosphere–ocean system. *Journal of Quantitative Spectroscopy and Radiation Transfer*, *41*, 483–494.

Doerffer, R., & Schiller, H. (2007). The MERIS Case 2 water algorithm. *International Journal of Remote Sensing*, *28*(3–4), 517–535.

Frette, O., Stamnes, J. J., & Stamnes, K. (1998). Optical remote sensing of marine constituents in coastal waters: A feasibility study. *Applied Optics*, *37*(36), 8318–8326.

Gilbert, J. C., & Lemaréchal, C. (1989). Some numerical experiments with variable-storage quasi-Newton algorithms. *Mathematical Programming*, *45*, 407–435.

Gordon, H. R. (1997). Atmospheric correction of ocean color imagery in the Earth Observing System era. *Journal of Geophysical Research*, *102*, 17081–17106.

Jamet, C., Moulin, C., & Thiria, S. (2004). Monitoring aerosol optical properties over the Mediterranean from SeaWiFS images using a neural network inversion. *Geophysical Research Letters*, *31*(13).

Jamet, C., Thiria, S., Moulin, C., & Crepon, M. (2005). Use of a neuro-variational inversion for retrieving oceanic and atmospheric constituents from ocean color imagery: A feasibility study. *Journal of Atmospheric and Oceanic Technology*, *22*(4), 460–475.

Kou, L., Labrie, D., & Chylek, P. (1993). Refractive indices of water and ice in the 0.65-μm to 2.5-μm spectral range. *Applied Optics*, *32*, 3531–3540.

Kourafalou, V. (2001). River plume development in semi-enclosed Mediterranean regions: North Adriatic Sea and north Aegean Sea. *Journal of Marine Systems*, *30*(3–4), 181–205.

Kuchinke, C. P., Gordon, H. R., & Franz, B. A. (2009). Spectral optimization for constituent retrieval in Case 2 waters I: Implementation and performance. *Remote Sensing of Environment*, *113*(3), 571–587.

Lee, Z. (2003). *Models, parameters, and approaches that are used to generate wide range of absorption and backscattering spectra.* : Report of the Ocean Color Algorithm Working Group., International Ocean Colour Coordinating Group (IOCCG).

Loisel, H., & Morel, A. (2001). Non-isotropy of the upward radiance field in typical coastal (Case 2) waters. *International Journal of Remote Sensing*, *22*(2–3), 275–295.

Mélin, F., & Zibordi, G. (2005). Aerosol variability in the Po Valley analyzed from automated optical measurements. *Geophysical Research Letters*, *32*(L03810), 1–4 (doi:).

Moore, G. F., Aiken, J., & Lavender, S. J. (1999). The atmospheric correction of water colour and the quantitative retrieval of suspended particulate matter in Case II waters: Application to MERIS. *International Journal of Remote Sensing*, *20*(9), 1713–1733.

Morel, A., & Prieur, L. (1977). Analysis of variations in ocean color. *Limnology and Oceanography*, *22*, 709–722.

Moulin, C., Gordon, H. R., Chomko, R., Banzon, V. F., & Evans, R. H. (2001). Atmospheric correction of ocean color imagery through thick layers of Saharan dust. *Geophysical Research Letters*, *28*, 5–8.

Pope, R. M., & Fry, E. S. (1997). Absorption spectrum (380–700 nm) of pure water. II. Integrating cavity measurements. *Applied Optics*, *36*, 8710–8723.

Rast, M., Bezy, J. L., & Bruzzi, S. (1999). The ESA medium resolution imaging spectrometer MERIS: A review of the instrument and its mission. *International Journal of Remote Sensing*, *20*(9), 1681–1702.

Ruddick, K., De Cauwer, V., Park, Y. -J., & Moore, G. (2006). Seaborne measurements of near infrared water-leaving reflectance: The similarity spectrum for turbid waters. *Limnology and Oceanography*, *51*(2), 1167–1179.

Ruddick, K., Ovidio, F., & Rijkeboer, M. (2000). Atmospheric correction of SeaWiFS imagery over turbid coastal waters: A practical method. *Remote Sensing of Environment*, *74*, 195–206.

Sathyendranath, S. (2000). *Remote sensing of ocean colour in coastal, and other optically-complex waters.* Report No. 3 of the Ocean Color Algorithm Working Group. : International Ocean Colour Coordinating Group (IOCCG).

Schroeder, T., Behnert, I., Schaale, M., Fischer, J., & Doerffer, R. (2007). Atmospheric correction algorithm for MERIS above case-2 waters. *International Journal of Remote Sensing*, *28*(7), 1469–1486.

Sydor, M., Gould, R. W., Arnone, R. A., Haltrim, V. I., & Goode, W. (2002). Spectral analysis of bulk reflectance from coastal waters: Deconvolution of diffuse spectra due to scattering and absorption by coastal water. *Journal of Coastal Research*, *18*, 352–361.

Talagrand, O., & Courtier, P. (1987). Variational assimilation of meteorological observations with the adjoint vorticity equation. I: Theory. *Quarterly Journal of the Royal Meteorological Society*, *113*, 1311–1328.

Thiria, S., Mejia, C., Badran, F., & Crépon, M. (1993). A neural network approach for modeling nonlinear transfer functions: Application for wind retrieval from spaceborne scatterometer data. *Journal of Geophysical Research*, *98*(C12), 22827–22841.

Umgiesser, G., & Bergamasco, A. (2002). *The spreading of the Po Plume and the Italian Coastal Current.* Consiglio Nazionale delle Ricerche, Italy: ISDGM.

Vidot, J., Santer, R., & Aznay, O. (2008). Evaluation of the MERIS aerosol product over land with AERONET. *Atmospheric Chemistry and Physics*, *8*, 7603–7617.

Zibordi, G., Holben, B., Hooker, S. B., Mélin, F., Berthon, J. -F., Slutsker, I., et al. (2006a). A network for standardized ocean color validation measurements. *EOS. Transactions*, *87*, 293–297.

Zibordi, G., Melin, F., & Berthon, J. F. (2006b). A time-series of above-water radiometric measurements for coastal water monitoring and remote sensing product validation. *IEEE Geoscience and Remote Sensing Letters*, *3*, 120–124.